The jet characteristics of bubbles near mixed boundaries

Li, SM; Zhang, A. M.; Wang, Qian; Li, S

DOI:
10.1063/1.5112049

The jet characteristics of bubbles near mixed boundaries

Cite as: Phys. Fluids **31**, 107105 (2019); https://doi.org/10.1063/1.5112049
Submitted: 03 June 2019 . Accepted: 25 September 2019 . Published Online: 10 October 2019

S.-M. Li (李世民), A.-M. Zhang (张阿漫), Q. X. Wang, and S. Zhang (张帅)

Physics of Fluids ARTICLE scitation.org/journal/phf

The jet characteristics of bubbles near mixed boundaries

Cite as: Phys. Fluids 31, 107105 (2019); doi: 10.1063/1.5112049
Submitted: 3 June 2019 • Accepted: 25 September 2019 •
Published Online: 10 October 2019

S.-M. Li (李世民),[1] A.-M. Zhang (张阿漫),[1,a)] Q. X. Wang,[2] and S. Zhang (张帅)[1]

AFFILIATIONS

[1]College of Shipbuilding Engineering, Harbin Engineering University, Harbin 150001, People's Republic of China
[2]School of Mathematics, University of Birmingham, Edgbaston, Birmingham, United Kingdom

[a)]**Author to whom correspondence should be addressed:** zhangaman@hrbeu.edu.cn

ABSTRACT

The jet characteristics of bubbles near mixed boundaries have been the focus of research in many fields. As the associated parameters are complicated, relatively few reports have been published. In this paper, a numerical model is established by considering the influence of the free surface and a mutual vertical wall using the boundary element method. To determine the jet characteristics of collapsing bubbles in different areas, two nondimensional parameters must be investigated: the distance γ_v from the bubble to the vertical wall and the distance γ_h from the bubble to the horizontal wall. At the same time, the buoyancy parameter δ cannot be ignored. First, the jet characteristics under an infinite vertical solid wall are discussed; furthermore, the jet direction in the stage of collapsing bubble under combined boundaries without buoyancy is studied, and we find that the variation amplitude of the jet angle changes with the free surface. Considering the buoyancy, we then divide the total area into six regions with different ranges of jet angle under small buoyancy values, allowing the significant effect of buoyancy to be studied as δ increases. In addition, we study the jet velocity qualitatively under the condition of negligible buoyancy and find that a peak jet velocity may exist at mid water depths.

I. INTRODUCTION

The motion of bubbles under complex boundaries has been a central issue of research in many fields.[1–6] Studies on the movement of bubbles near mixed boundaries are of great importance in engineering and scientific research, such as the cavitation bubbles generated on propeller tubes,[7,8] shallow coastal explosions used to unblock channels,[9] air gun bubbles,[10–12] and bubble dynamics in water tanks.[13–15] All of these applications consider the similar scenario of bubble dynamics near complex boundaries. In such scenarios, a high-speed liquid jet forms under the action of buoyancy or because of the boundaries. This jet impacts on the surrounding fields or boundaries, but the jet direction is difficult to predict. However, the jet direction can significantly affect the position of the bubble impact, and so the study of the jet characteristics in such conditions seems essential.

Representatively, the explosion bubble used to unblock the channel in shallow water is affected by several boundaries including the bottom, the shore, and the free surface. This application could be simplified to the scenario studied in this paper. The Bjerknes forces[16,17] acting on the explosion bubble from the horizontal wall and the free surface are both downward, but it is difficult to judge which one is greater. Simultaneously, the scale of the bubble generated by underwater explosion is large, leading to the inevitable effect of buoyancy. In addition, the vertical wall also will influence the bubble in a certain range. All of these considerations lead to the complexity of the present study, and so it is difficult to determine in which area the bubble jet will impact which boundary. Besides, a cavitation bubble in a propeller tube, an air gun bubble near the island, and an electric spark bubble in a water tank all face the similar problems. Once we have a clear understanding of the basic issue mentioned in this paper, we could use the associated conclusions to guide related research and engineering.

There are two main problems to solve in these applications. The first is the interaction between the bubble and the combined complex boundaries; the second is the jet characteristics of

bubbles at different distances from the boundary. To solve these problems, there has been considerable research on bubble jets under the Bjerknes force and buoyancy. As early as the 1980s, Blake[16,17] used a boundary integral method to study the joint effect of buoyancy and the distance to the boundary on the jet characteristics, and this work has a great guiding role on the present research. Cui[18] conducted an experimental study on the motion of bubbles between a free surface and a horizontal wall and found that the bubble jet points toward the wall. However, the buoyancy effect was not thoroughly studied. Wang and Chu[19] studied the features of bubble motion at the corner of two walls, but there has been little analysis of the bubble jet direction. In terms of numerical simulations, significant efforts have been made in recent years.[20–26] Wang[27] analyzed the motion of bubbles with a free surface near an inclined solid wall with the boundary element method (BEM), which provides a reference for studying the interaction between the bubble and mixed boundaries. However, this work assumed that the wall is semi-infinite, with no influence from a bottom surface. As for some other simulation methods such as the finite volume method,[28–30] front tracking method,[31] lattice Boltzmann method,[32] and so on, there also exists a lot of valuable works on bubble dynamics. Tagawa[33] conducted some research about the bubble dynamics and jet characteristics of bubbles in the corner and accurately predicted the jet direction, but the influence of the free surface was not considered. As for the complicated situations, Cui[34] studied the interaction between the bubble and complex boundaries, finding lots of interesting laws governing the motion of bubbles with rare analysis in the jet characteristics. In addition, Maiga[35] conducted works on the bubble theory, the conditions being too simple.

From the above discussion, it is clear that bubble dynamics under a single boundary have been intensively studied by researchers in recent decades, but little attention has been paid to the jet characteristics of collapsing bubbles under the combined effects of mixed boundaries. In this paper, the numerical model used to simulate bubbles near mixed boundaries is first established using a boundary element method (BEM). We then present two typical experiments that verify our numerical model. Studies on the collapsing bubble jet under a free surface or horizontal solid wall have generated many important results, but the influence on the jet direction of a vertical wall has rarely been reported. Thus, in this paper, the bubble jet is examined under the influence of a vertical solid wall, and a jump in the jet angle near the wall is observed and analyzed. We then discuss the joint influence of the buoyancy parameter and the distance between the bubble and the boundary on the bubble jet. By analyzing and summarizing the calculation results, we show that the bubble jet tends to point downward in most areas without buoyancy, but under small buoyancy values, the situation becomes complex. We therefore divide the area into six parts with different jet directions. As the buoyancy increases, the effect of the other boundaries becomes relatively small. When the dimensionless buoyancy parameter reaches 0.6, the influence of the boundaries becomes negligible. In order to reveal the law of jet impacts near the wall, in the case of negligible buoyancy, we also study the velocity of the bubble jet in qualitative terms, verifying some conclusions from previous research,[19,36] and find that a peak jet velocity exists approximately equidistant from the free surface and the bottom.

II. NUMERICAL MODEL

A. Coordinate system and parameters

The working conditions assumed for this study are shown in simplified form in Fig. 1. A Cartesian coordinate system is created as shown in the picture. The origin of the coordinate system is at the initial center position of the bubble, the x-axis points horizontally to the vertical wall, the z-axis points vertically upward, and the directions of the x-axis, y-axis, and z-axis conform to the right-hand rule. There are three distance parameters in the figure: the water depth H, the distance d_v between the initial center position of the bubble and the vertical wall, and the distance d_h between the initial center position of the bubble and the horizontal wall.

In terms of the water depth, if the bubble is too deep, the influence of the free surface cannot be considered; conversely, if the depth is too small, the nonlinear coupling[15] between the bubble and the free surface would require a thorough treatment, which is beyond the scope of the present study. According to Blake's criterion,[17] once the water depth is more than six times the maximum radius of the bubble, the effect of the free surface can be offset by a small amount of buoyancy. Thus, in this paper, the initial water depth is taken to be six times the maximum radius of the bubble. Above this, the distance d_h could represent two physical features, namely, the distance between the bubble and the bottom or the distance between the bubble and the free surface (the sum of the two distances is fixed).

B. Basic theory of BEM and definition of feature parameters

Underwater explosion bubbles and high-pressure air gun bubbles can be considered as nonstick, inviscid, irrotational, nonrotating, and incompressible fluids, at least in the first cycle of oscillation.[11,21,37] Therefore, based on potential flow theory, the fluid velocity potential needs to satisfy the integral equation as follows:

$$\lambda(\mathbf{p})\varphi(\mathbf{p}) = \iint_s \left[G(\mathbf{p},\mathbf{q}) \frac{\partial \varphi(\mathbf{q})}{\partial n(\mathbf{q})} - \frac{\partial G(\mathbf{p},\mathbf{q})}{\partial n(\mathbf{q})} \varphi(\mathbf{q}) \right] ds, \quad (2.1)$$

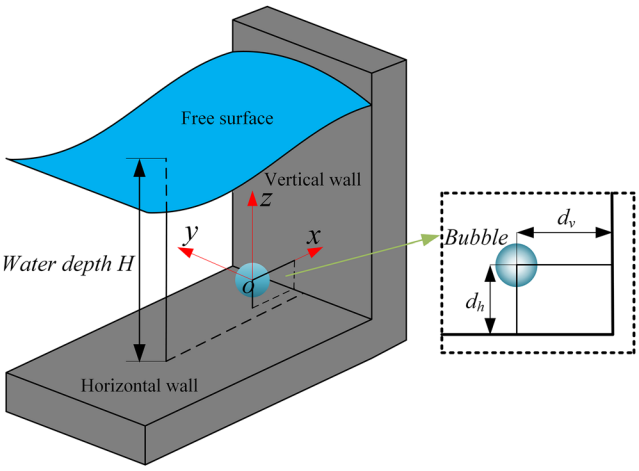

FIG. 1. Schematic diagram of required research conditions.

where $\mathbf{p}$ is the vector of field points, $\mathbf{q}$ is the vector of source points, $\varphi(\mathbf{p})$ and $\varphi(\mathbf{q})$ are the corresponding velocity potentials, $G(\mathbf{p}, \mathbf{q}) = |\mathbf{p} - \mathbf{q}|^{-1}$ is Green's function, $n(\mathbf{q})$ denotes the unit normal vector pointing to the fluid field outside the bubble, $\lambda(\mathbf{p})$ is a parameter denoting solid angles, and s is the area of the bubble surface.

To derive the general conventions, all of the parameters need to be dimensionless.[38] The reference pressure, length, and density are p_∞ (hydrostatic pressure of the bubble's center position), R_m (the maximum radius of the bubble), and ρ (the density of the fluid), respectively. Other parameters could be dimensionless based on these three fundamental parameters. Therefore, reference velocity, time, and potential of velocity can be written as $(p_\infty/\rho)^{1/2}$, $R_m(\rho/p_\infty)^{1/2}$, and $R_m(p_\infty/\rho)^{1/2}$, respectively.[39] In addition, three important dimensionless parameters[16,17,27,39] mainly used in this paper are defined as

$$\delta = (\rho g R_m/p_\infty)^{1/2}, \quad \gamma_v = \frac{d_v}{R_m}, \quad \gamma_h = \frac{d_h}{R_m}, \tag{2.2}$$

where δ is the buoyancy parameter, which represents the effect of the buoyancy, γ_v is the dimensionless bubble–vertical wall distance, and γ_h is the dimensionless bubble–horizontal wall distance.

At the boundaries, the dynamic boundary condition could be written as (2.3) (dimensionless Bernoulli equation),[39] with the pressure on the free surface set to atmospheric pressure. In this paper, we do not consider the flow of gas inside the bubble, and so based on the adiabatic assumption, the gas pressure inside the bubble[40,41] can be expressed as in the following equations:

$$\frac{\partial \varphi'}{\partial t} = 1 - P' + \delta^2 z' - \frac{1}{2}|\nabla \varphi'|^2, \tag{2.3}$$

$$P' = \varepsilon \left(\frac{V'_0}{V'}\right)^{\gamma}, \tag{2.4}$$

where prime symbols denote dimensionless parameters, V_0 is the volume of the bubble at inception, V denotes its present volume, γ is the ratio of heats, taken as 1.25 for bubbles generated by collapsing,[39] and ε is a strength parameter representing the initial pressure inside the bubble.

The bubble and the boundaries are discretized according to Zhang *et al.*[42] and Li *et al.*[41] The process of bubble motion is solved by the time advancement method, where the normal velocity of the bubble surface is acquired by Eq. (2.1), and the true velocity of each node on the boundary is then obtained by the finite difference method. The Bernoulli equation is used to determine the velocity and position of the bubble surface node in the next time step. For the purpose of ensuring stable calculations, the time step must be strictly controlled. In this paper, the time step is expressed as

$$\Delta t = \min\left\{\Delta t_0, \frac{\Delta \varphi}{\max\left(\left|\frac{d\varphi}{dt}\right|\right)}\right\}, \tag{2.5}$$

where Δt_0 is set to prevent the time step exceeding a certain value and $\Delta\varphi$ is the change in velocity potential between adjacent time steps.

C. 3D vortex model

After the bubble jet impacts the surface of bubble, the condition becomes very complicated. The domain assumes a ring shape, and the above theory cannot solve the problem. The vortex model has been developed over many years for this condition,[11,22,43,44] and in this paper, we adopt a 3D vortex model to update the node information. First, the velocity potential φ can be regarded as the sum of the potentials of the ring φ_v and the residual φ_r.[5,22,27,39] The induced velocity of the ring u_v can then be acquired using Biot–Savart's law,

$$\varphi = \varphi_v + \varphi_r, \tag{2.6}$$

$$u_v = \frac{K}{4\pi} \oint_C \frac{\boldsymbol{r} \times d\boldsymbol{l}}{|\boldsymbol{r}|^3}, \tag{2.7}$$

where dl is a small element on the vortex, $\boldsymbol{r}$ is the vector from the element to the node on the surface of the bubble, C is the curved line denoting the vortex, and K is the jump in the potential on the impacted node, which is calculated using a previous result.[39] In three dimensions, it is very complex to solve the above equation directly, and so a semianalytic method is adopted. For the nodes on the surface of the bubble, the velocity potential[39,42,44] above the vortex can be written as

$$\varphi_v = \frac{K}{4\pi} \oint_C \left(\frac{r_z}{|\boldsymbol{r}|} - 1\right) \frac{1}{r_z^2} [\boldsymbol{e_z} \cdot (d\boldsymbol{l} \times \boldsymbol{r})] \tag{2.8}$$

and that underneath the vortex can be expressed as

$$\varphi_v = \frac{K}{4\pi} \oint_C \left(\frac{r_z}{|\boldsymbol{r}|} + 1\right) \frac{1}{r_z^2} [\boldsymbol{e_z} \cdot (d\boldsymbol{l} \times \boldsymbol{r})], \tag{2.9}$$

where the subscripts "r" and "z" represent the radial direction and the direction of the z-axis. We refer to the work of Zhang and Liu[39] to update the position and velocity of the nodes.

D. Treatment of the speed of junction nodes

Through the above calculations, the normal velocity of the nodes on the free surface and the junction, and the velocity potential of the wall nodes, can be obtained. Furthermore, the actual velocity of the nodes can be acquired from the difference relationship between the unit normal velocity and the velocity potential. However, the velocity of junction points cannot satisfy two boundary conditions (wall and free surface) at the same time, as this may lead to some distortion of the grids and cause the calculations to fail. Hence, in this paper, the velocity of the junction points is treated in the following way.

We define the speed of a junction point perpendicular to the solid wall as v_{nw}. To meet the boundary conditions of the solid wall, v_{nw} is fixed at 0; according to the continuity of the fluid, the speed in the other two directions can be updated by averaging the speeds of the surrounding nodes according to

$$v_y = \alpha_1 \frac{1}{n_f} \sum_{i=1}^{n_f} v_{yf} + \beta_1 \frac{1}{n_j} \sum_{i=1}^{n_j} v_{zj}, \tag{2.10}$$

$$v_z = \alpha_2 \frac{1}{n_f} \sum_{i=1}^{n_f} v_{zf} + \beta_2 \frac{1}{n_j} \sum_{i=1}^{n_j} v_{zj}, \tag{2.11}$$

where v_y and v_z denote the velocity of the junction node in the y and z directions, respectively, n_f and n_j denote the number of nodes on the free surface and the junction surrounding the junction node, respectively, and α_1, α_2, β_1, β_2 are weighting factors. The nodes at the junction must satisfy two boundary conditions, whereas those on the free surface satisfy only the free surface boundary condition. In fact, the junction nodes may be affected by the friction between the fluid and the wall, and so the velocity of the junction nodes may be considered to approach that of the nodes on the free surface. (In this paper, when the bubble is close to the junction nodes, α_1 and α_2 are set to 0.3, and β_1 and β_2 are set to 0.7; otherwise, α_1, α_2, β_1, β_2 are all set to 0.5.)

E. Definition of direction of the bubble jet

The grids are optimized in the manner described by Zhang and Liu.[39] To describe the direction of the bubble jet in quantitative terms, the jet direction can be delimited as follows:

As shown in Fig. 2, node o is that with the highest speed on the surface of the bubble before the jet impact. The jet angle $\boldsymbol{n}_{i\ i+5}$ is obtained by calculating the normal vector of the closed curve formed by the nodes around node o. The calculation formula is

$$\alpha = w_1 \frac{1}{n_1} \sum_{i=1}^{n_1} \arccos\left[\left(\boldsymbol{n}_{i'i'+2} \times \boldsymbol{n}_{i'i'+4}\right) \cdot \boldsymbol{n}_x\right] + w_2 \frac{1}{n_2} \sum_{i=1}^{n_2} \arccos\left[\left(\boldsymbol{n}_{ii+5} \times \boldsymbol{n}_{ii+8}\right) \cdot \boldsymbol{n}_x\right], \tag{2.12}$$

where n_1 and n_2 denote the number of nodes surrounding node o on the first and second laps, respectively, $\boldsymbol{n}_{i\ i+5}$ is the vector from node i to node $i + 5$, $\boldsymbol{n}_x$ is the unit vector in the direction of the x-axis, and w_1, w_2 are weighting factors ($w_1 + w_2 = 1$) representing the proportion of nodes on the first and second laps, respectively.

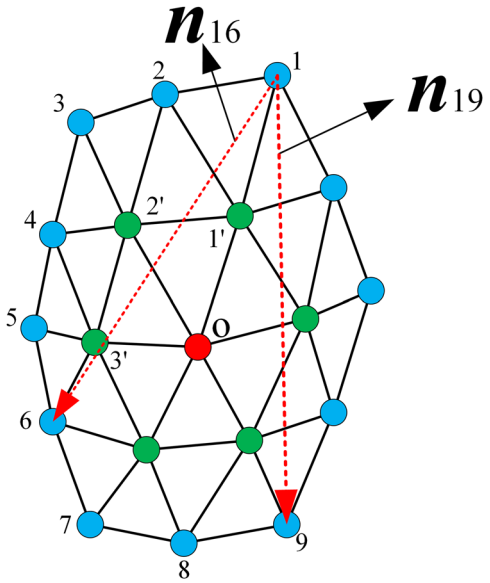

FIG. 2. Topology of grids.

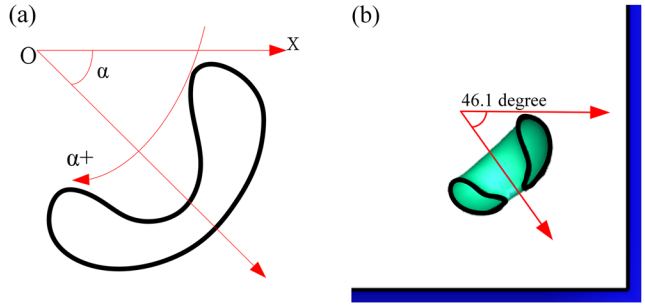

FIG. 3. Definition and verification of jet angle. (a) Definition of jet angle. The arrow denotes the direction of increasing angle; (b) Verification of jet angle (γ_h = γ_v = 1.5, δ = 0).

As the jet is thin, the nodes close to node o attain a high velocity, and so the grid can easily become irregular. Thus, the normal vector of the closed curve formed by nodes surrounding node o on the second lap represents the jet direction better. Hence, w_2 is set to 0.7; for a wide jet, w_2 would be set to 0.4.

Taking the x-axis as the reference, the angle is positive when the jet rotates clockwise around this axis, as shown in Fig. 3(a); it is obvious that the jet of bubbles in the free field moves vertically upward[13,39] (that is, the real jet angle is −90° according to the definition of jet angle in this paper). Thus, we calculate the jet angle of the bubble in the free field (δ = 0.2) and find that the result is −92.6° which is generally consistent with the real jet angle. We then draw the jet angle calculated by the method of this paper in the picture under the conditions that γ_h = γ_v = 1.5, δ = 0. As shown in Fig. 3(b), the jet angle calculated in this paper represents the jet direction well.

III. VERIFICATION OF THE NUMERICAL MODEL

To verify the reliability of the numerical model, the calculation results given by the method of this paper are compared with the results of experiments. In the experiments, the bubble is formed by sparking with a wire electrode. Bubbles have been generated in this way for decades and are widely used in experiments to observe bubble dynamics.[13–15,45–51] We conducted experiments using the system described by Li,[37] as shown in Fig. 4. In the experiments, we use a high voltage (~670 V) to generate bubbles [$R_m \approx 11.5$ mm, so according to (2.2) and (2.3), the effect of buoyancy is negligible] and a high-speed camera to capture the bubble behavior. Two walls of the water tank form the corner geometry, and the water depth is set to 69.5 mm. In numerical simulations, the strength parameter ε has little influence on the shape of the bubbles,[52] and so its value can be selected arbitrarily. The initial radius of the bubbles can be acquired from the Rayleigh–Plesset equation[53] combined with (2.1) and (2.3); thus, in the present and subsequent studies, ε is set to 20, and the initial dimensionless radius is fixed at 0.2695.

First, we compared the shapes of bubble simulated by BEM with the experimental bubbles in two cases, as shown in Figs. 5 and 6. The bubble shape calculated using BEM coincides well with the experimental results before the jet impact, but in the collapse

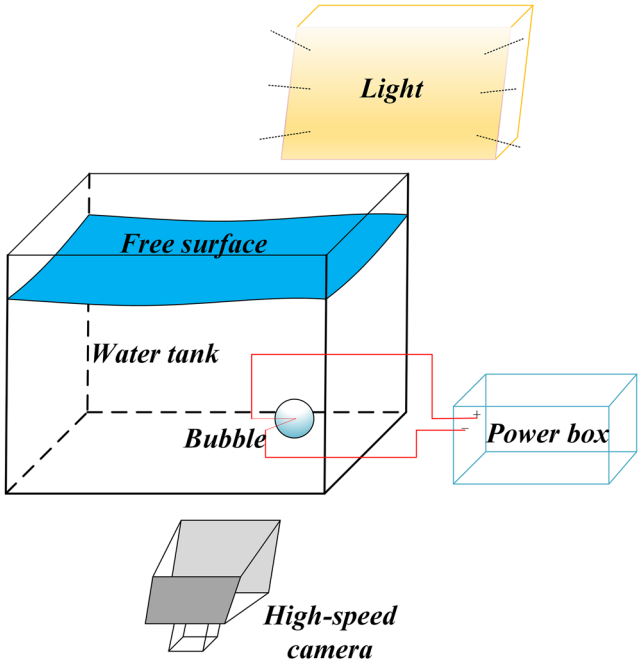

FIG. 4. Arrangement of devices for the experiment.

phase, the dimensionless times have some discrepancies. Specifically, the dimensionless time in the experiments is relatively longer than that in the numerical simulation. This may be the result of the smaller feature time $[R_m(\rho/P_\infty)^{1/2}$, where P_∞ is atmospheric pressure] selected as the experimental time scale, as well as some measurement errors. In addition, the experimental bubbles do not form instantly, whereas those in the simulation are generated instantaneously; this may be another reason for the discrepancies. There are also some slight differences in the size of the bubbles, which may result from the mismatch of dimensionless time between the experiments and simulation and the measurement errors.

Near the corner region, our numerical model reproduces the jet shape well before the jet impact. Under the action of the Bjerknes forces from two walls (the influence of the free surface is very small in this case), the bubble takes a nonspherical shape in the late stage of expansion. A jet pointing toward the corner then emerges, and the jet penetrates the bubble surface and collapses into the corner under the high speed of the liquid jet. In the case shown in Fig. 6, near the free surface and vertical wall, our numerical model recreates the motion of the bubble well until the jet impact. The Bjerknes force of the free surface then drives the upper part of the bubble surface to flatten, before a vertical downward jet gradually develops. At the same time, the left part of the bubble sinks to the right under the Bjerknes force of the wall. Note that the free surface rises constantly during this process as a result of the appearance of a region of high pressure,[17,54] and the friction between the wall and the water retards the upward movement of liquid close to the wall,[36] causing a turning near the junction of the free surface and the wall [see frames (c)–(h) in Fig. 6]. In the calculation process, stability is maintained until the moment of jet impact.

Besides the jet shape and jet angle of the bubble, the velocity of the bubble jet is also of interest. Thus, we conduct several experiments to verify the jet velocity; the corresponding comparison between numerical and experimental results will be presented in a Sec. IV.

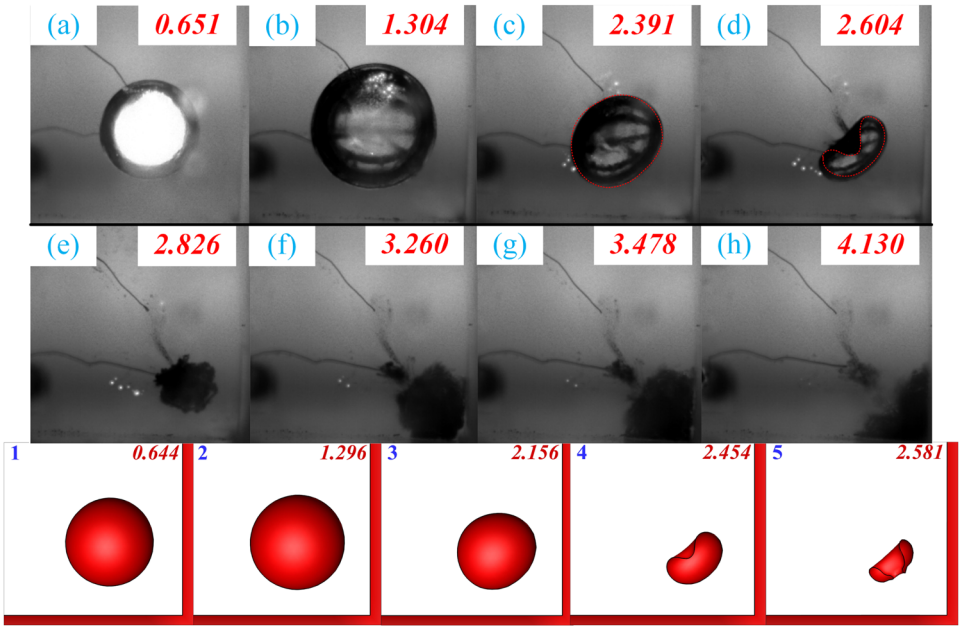

FIG. 5. Comparison of the experiments with the numerical results near the corner (γ_v = 1.5, γ_h = 1.5). The dimensionless times in the experiments and simulations are denoted in the corner of each image; frames (1)–(4) of the simulations correspond to frames (a)–(d) in the experiments, and the results of frames (3)–(4) in the simulations are also depicted in frames (c)–(d) of the experiments; the other parameters in the experiments are R_m = 11.5 mm, H = 69.5 mm, d_v = 17.3 mm, and d_h = 17.3 mm. The frames (e)–(h) of the experiments shows the later bubble collapsing stage, in which the bubble expands again and migrates towards the corner.

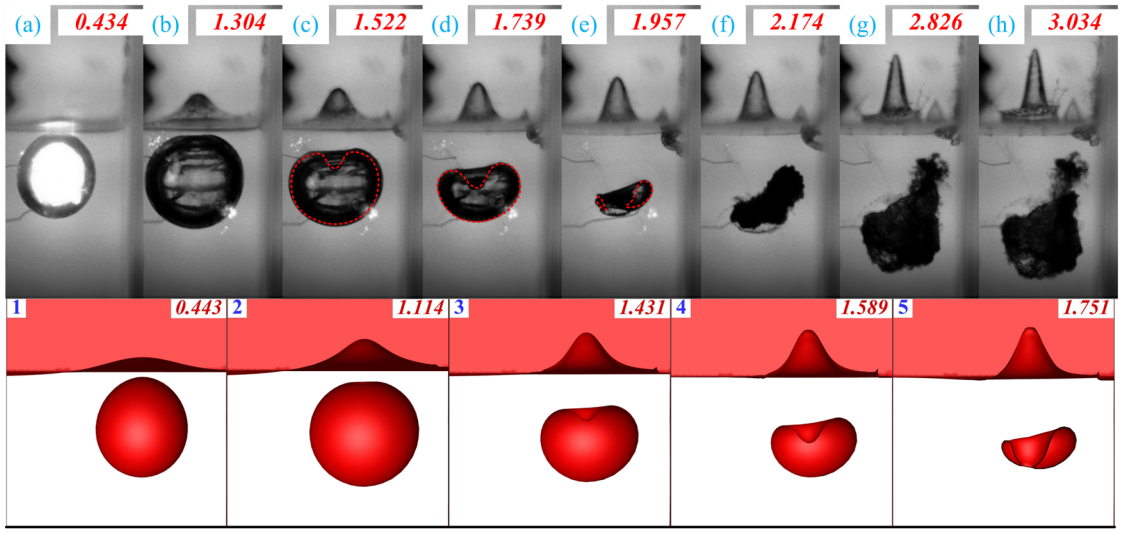

FIG. 6. Comparison of the experiments with the numerical results at corresponding dimensionless times near the free surface (γ_v = 1.5, γ_h = 5.0). The dimensionless times in the experiments and simulations are denoted in the corner of each image; frames (1)–(5) in the simulations correspond to frames (a)–(e) in the experiments, and the results of frames (3)–(5) in the simulations are also depicted in frames (c)–(e) of the experiments; the other parameters in the experiments are R_m = 11.5 mm, H = 69.5 mm, d_v = 17.3 mm, and d_h = 57.7 mm. The frames (f)–(h) of the experiments shows the later bubble collapsing stage, in which the bubble expands again and travels downwards.

IV. ANALYSIS OF RESULTS

A. Jet characteristics of bubbles under the influence of infinite vertical wall

To study the range of influence of the vertical wall on the bubble jet direction, the bubble jet shape under different distance parameters γ_v was first simulated using the method described in Sec. II. The evolution of the jet and the cause of its formation have been studied in depth,[2,5,55] and so we focus on the law governing the jet direction. In the simulation, we place the single infinite vertical wall on the right side of the bubble so that we could compare the results between the conditions of this section and Sec. IV B. As shown in Fig. 7, with δ = 0.2, the bubble is jetted upward while its left part is affected by the vertical solid wall. As γ_v increases, the effect on the left part of the bubble gradually reduces; when γ_v = 5.5, the shape of the collapsing bubble is very close to that in the free field, and the jet points almost vertical upward; at this time, the solid wall has a negligible effect on the bubble.

Figure 8 depicts the change in the jet angle with respect to γ_v for different values of δ. The effect of buoyancy on the jet shape of the bubble is obvious. When δ = 0.4, the effect of the wall on the bubble is significantly smaller than when δ = 0.2, and when γ_v approaches ~4.5, the jet angle becomes greater than 85° (almost vertical). When δ = 0.6, the range of influence of the vertical wall on the bubble jet direction continues to decrease, and the jet direction is no longer affected by the vertical wall once γ_v reaches ~3.5. Hence, as the buoyancy parameter δ increases, the vertical wall affects the direction of the jet over a shorter distance. The results suggest that the range of influence decreases linearly with the increase in δ, but the specific relationship between δ and the range is beyond the scope of this study, as it would require a large number of simulations and theoretical analysis.

A key feature to note is that the jet angle jumps when the bubble is close to the vertical wall, as the red arrow in Fig. 8 shows. When the bubble is close to the wall, the Bjerknes force of the wall is larger, causing the liquid jet to point toward the wall. However, the results do not conform to this regularity, i.e., near the vertical wall (γ_v = 1.0, 1.5), the liquid jet tends to point upward rather than at the wall. This phenomenon can be attributed to the definition of the jet direction. In the associated literature,[19,33,56] researchers often judge

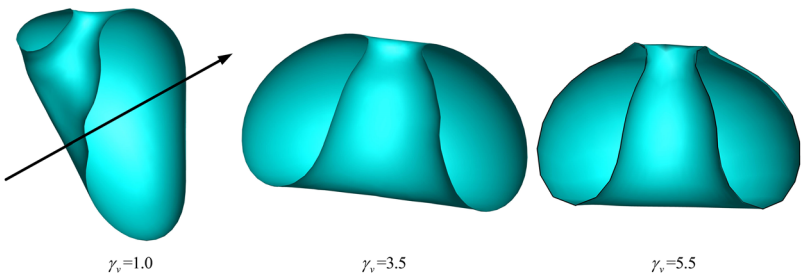

FIG. 7. Jet shape at different γ_v with δ = 0.2. The corresponding dimensionless moments are 2.332, 2.201, and 2.176, respectively; corresponding dimensionless distances are 1.0, 3.5, and 5.5, respectively.

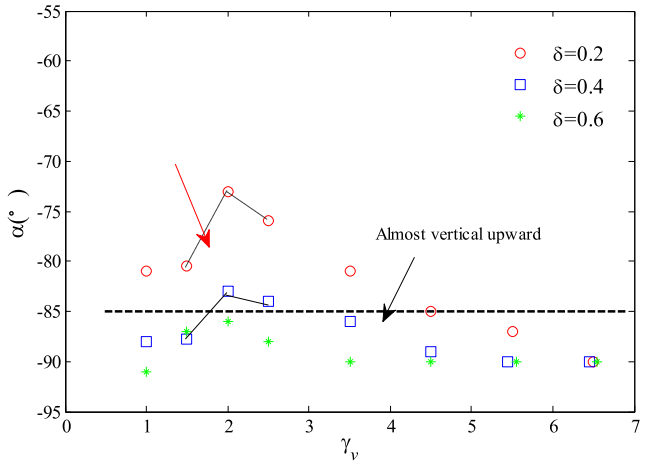

FIG. 8. Jet angles of bubble with respect to γ_v for different values of δ. The different symbols denote different dimensionless buoyancy parameters, i.e., red circles, blue squares, and green crosses denote jet angle when δ equals 0.2, 0.4, and 0.6, respectively. The area below the dashed line represents an almost-upward jet.

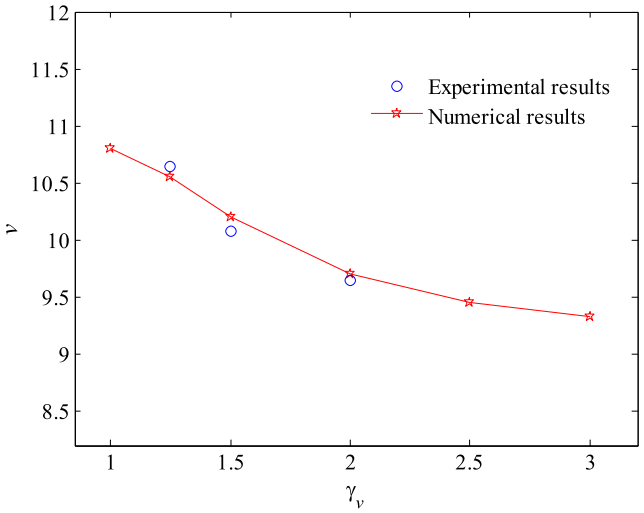

FIG. 9. Jet velocities changing with γ_v in experiments ($\delta \approx 0$) and simulation ($\delta = 0$). v is the dimensionless velocity of the jet tip; the blue circle represents the velocity of the jet tip in experiments, and the red line denotes that in the numerical simulation.

the jet direction according to the profile of the bubble, because the limitations of experimental conditions prevent the liquid jet from being clearly captured. This may lead one to think that the jet direction of the bubble may be deduced from the curvature of the bubble surface, as shown by the black arrow in Fig. 7 (the first picture). However, when the bubble is very close to the vertical wall, the very existence of the wall prevents the bubble from expanding to the extent it would in the free field, and the part of the bubble surface near the vertical wall is retarded during the expansion stage, resulting in a decrease in the liquid velocity between the bubble and the wall. Therefore, the liquid pressure in that region becomes relatively high, leading to a decrease in the pressure difference between the left and right sides of the bubble. Moreover, if the buoyancy is nonzero, the force in the vertical direction will strengthen, causing the liquid jet to be directed upward.

When the bubble is relatively far from the wall, the bubble is subjected to the Bjerknes force from the wall as well as the buoyancy. With the increase in γ_v, the Bjerknes force decreases, and until the bubble keeps away from the wall to an enough distance, the liquid jet is directed upward because of the negligible Bjerknes force. Therefore, when the bubble is very close to the wall or far from the wall, the liquid jet always tends to be directed upward, causing a jump of the values of jet angles. We can see that a peak in the absolute value of the jet angle appears at $\gamma_v \approx 2.0$ because it is at this distance that the bubble would not be prevented from expanding by the wall obviously. With the increase of the buoyancy, the liquid jet has a greater possibility to point upward, causing the jump amplitude to decrease.

As for the velocity of the bubble jet, we discuss this in combination with the experimental results shown in Fig. 9. The jet velocity in the experiments was obtained in the following way. Two relatively clear adjacent pictures in the collapse phase of the bubble were identified, and the displacement of the jet tip between the two frames was determined. Finally, the ratio of the displacement to the corresponding time interval was computed. As shown in Fig. 9, the jet velocity obtained by the experiments is very close to the numerical results (to within acceptable error). The reason for the slight error is that the jet velocity in the numerical simulation is the instantaneous speed of the jet tip at a point, whereas that in the experiments was obtained by the above method, and thus represents the average velocity of the jet tip during the corresponding time interval. With an increase in the dimensionless distance, the jet speed decreases until γ_v reaches a value of 3; when γ_v is greater than 3, no obvious jet could be simulated due to the small effect of the vertical wall under the condition $\delta = 0$.

B. Jet characteristic of bubbles under the influence of the mixed boundary

1. Jet characteristics of bubbles without buoyancy

To study the influence of the combined boundary on the bubble jet, this section first excludes the influence of buoyancy by setting δ to 0 in the calculation. Thus, we concentrate on the influence of the distance between the bubble and the boundaries on the bubble jet direction. The working condition is set as Fig. 1. The bubble jet directions without buoyancy for different values of γ_v and γ_h are illustrated in Fig. 10. The Bjerknes force from the free surface acts in the downward direction, that is, it drives the bubble away from the free surface. The Bjerknes force from the wall causes the bubble to approach the wall. Therefore, in this case, the bubble is only subjected to the downward Bjerknes force in the vertical direction, leading to an oblique downward jet (jet angles are positive), as shown by the computational results in Fig. 10. When the γ_h reaches 4.0, as a result of the small distance between the bubble and free surface, strong nonlinear interaction[6] between them always makes the bubble generate a downward jet no matter how close the bubble is to the vertical wall. Even though the vertical wall exert an extraordinary impact on the bubble, the high pressure[15,57] between the bubble and

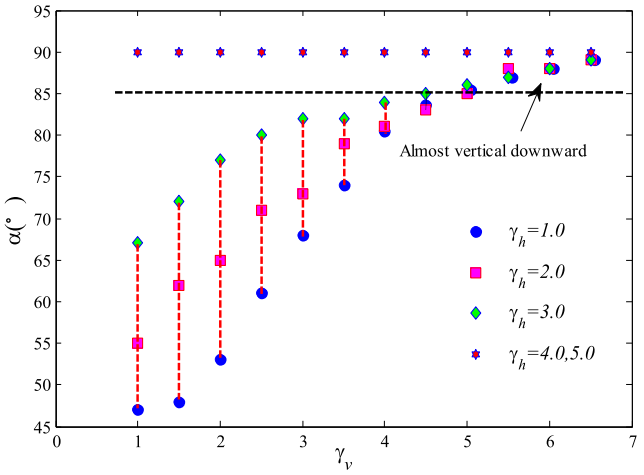

FIG. 10. Jet angles changing with γ_v under the condition of different γ_h. The dimensionless buoyancy parameter δ = 0; four different symbols denotes different dimensionless distance parameters, i.e., blue solid circles, pink solid squares, green solid diamonds, and pink stars denote jet angles when γ_h is equal to 1.0, 2.0, 3.0, and 4.0 (5.0), respectively; the area above the dashed line represents an almost-downward jet. Note that γ_h represents two distances, namely, the distance between the bubble and the horizontal wall, and the distance between the bubble and the free surface, that is, the dimensionless distance between the initial bubble and the free surface is 5.0, 4.0, 3.0, and 2.0 (1.0) when γ_h equals 1.0, 2.0, 3.0, and 4.0 (5.0), respectively.

the free surface would also drive the liquid jet directed downward, as the condition γ_h = 4.0 (5.0) in Fig. 10.

As γ_h increases at fixed γ_v, the jet angle gradually increases, reaching 90° when the bubble approaches the free surface with a high pressure zone forming beneath the free surface;[54,57] this increase in the jet angle means the increase of the Bjerknes force in the vertical direction; so in a sense this may prove that the effect of the Bjerknes force from the free surface is greater than that of the bottom wall under the same conditions, which also may be deduced in the numerical simulations of Blake.[16,17] With an increase in γ_v at fixed γ_h, the Bjerknes force exerted on the bubble in the vertical direction is constant, but that in the horizontal direction decreases, causing the joint force to rotate clockwise. Therefore, the jet angle gradually rotates clockwise with the increase of γ_v and eventually arrives to ~90° when the vertical wall is sufficiently far (about γ_v = 5.0) owing to the very small effect of the vertical wall. This increase in γ_v reduces the difference in jet angles for a fixed γ_v, as shown by the vertical red dotted lines in Fig. 10. As an explanation, the bubbles are subjected to three different Bjerknes forces (from the free surface, bottom, and vertical wall), and so near the vertical wall there is a very obvious difference in the acceleration of the bubble for the same γ_v, while the downward Bjerknes force is dominant at large values of γ_v, resulting in the bubble jet pointing almost vertically downward at any γ_h. Under the condition δ = 0, the jet of bubbles in the whole area generally points vertically down when γ_v is greater than 5.0 under the effect of the free surface.[27,58]

As suggested by the above description, in this condition, the jet of bubbles tends to point downward (or obliquely downward), and so in order to study the characteristics of the bubble jet in depth, there is a need to discuss the jet velocities under different dimensionless distances. As shown in Fig. 11, our numerical model calculates the jet velocity well compared with the experiments. In the horizontal direction, near the corner, the velocity of the bubble jet peaks when γ_v is between 1.0 and 2.0, and as γ_v increases, it tends to decrease continuously. A similar result was observed by Wang and Chu.[19] In the vertical direction, the jet velocity near the free surface is higher than that close to the horizontal wall, which agrees with previous research.[36] According to the

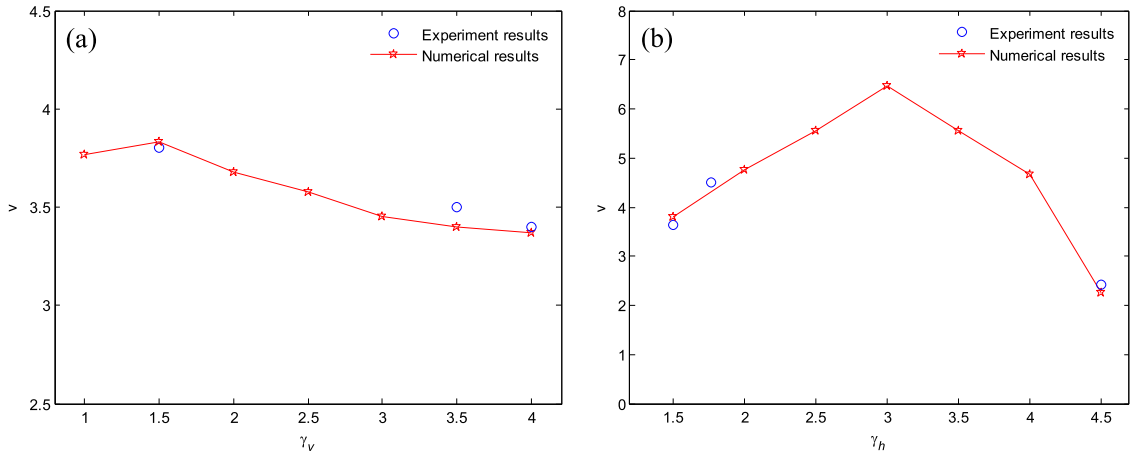

FIG. 11. Jet velocities under different dimensionless distances. (a) Jet velocities changing with γ_v in experiments ($\delta \approx 0$) and simulation (δ = 0) (γ_h = 1.5). v is the dimensionless velocity of the jet tip; the blue circle represents the velocity of the jet tip in the experiments, and the red line denotes that in the numerical simulation; (b) Jet velocities changing with γ_h in experiments ($\delta \approx 0$) and simulation (δ = 0) (γ_v = 1.5). v is the dimensionless velocity of the jet tip; the blue circle represents the velocity of the jet tip in the experiments, and the red line denotes that in the numerical simulation.

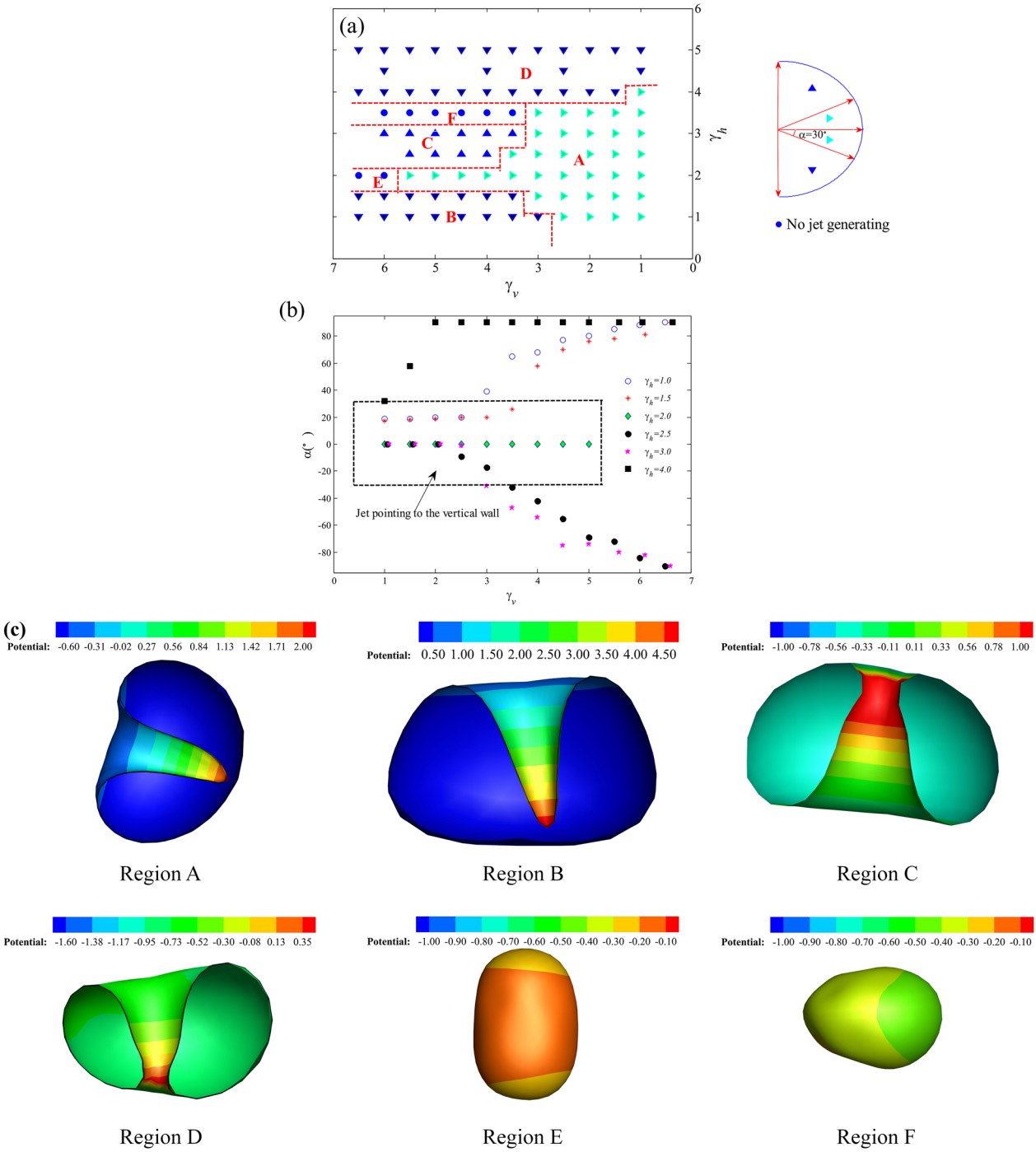

FIG. 12. Jet directions under different working conditions (δ = 0.2). (a) Six regions of different ranges of jet angles. The different symbols are defined in the right-hand panel. (b) Jet angles changing with γ_v under the condition of different γ_h. Six different symbols denote different dimensionless distance parameters between the bubble and horizontal wall; blue circles, red asterisks, green diamonds, black solid circles, pink pentagrams, and black squares denote the jet angle when γ_h equals 1.0, 1.5, 2.0, 2.5, 3.0, and 4.0, respectively; the box surrounded by the dashed line represents an jet almost pointing the vertical wall; similarly, the dimensionless distance between the initial bubble and free surface is 5.0, 4.5, 4.0, 3.5, 3.0, and 2.0 (1.0) when γ_h equals 1.0, 1.5, 2.0, 2.5, 3.0, and 4.0, respectively. (c) Typical bubble profiles in the stage of bubble collapsing from region A-F. Different colors denote different potentials, as presented on the top of the image; the corresponding dimensionless moments are 2.201, 2.301, 2.104, 2.016, 2.151, 2.021; the corresponding dimensionless distances: A(γ_v = 2, γ_h = 2.5), B(γ_v = 4.5, γ_h = 1.0), C(γ_v = 5.0, γ_h = 3.0), D(γ_v = 2.0, γ_h = 4.0), E(γ_v = 6.0, γ_h = 2.0), F(γ_v = 4.5, γ_h = 3.0).

numerical and experimental results in this paper, the jet velocity reaches a maximum when γ_h is ~3, i.e., the area of the isometric distance between the free surface and the bottom. In addition, note that the present jet velocity is much lower than with the vertical wall alone (Fig. 9).

2. Effect of buoyancy

a. Jet characteristics of bubbles under the action of small buoyancy ($\delta = 0.2$). Figure 12(a) illustrates the bubble jet direction when $\delta = 0.2$ in the whole area, and Fig. 12(c) gives the typical collapsing bubble profile in each region. In our simulations, we find that the parameter γ_v is almost greater than about 3.0 or more when the angle between the jet direction and the x-axis reaches about 30°. At $\gamma_v > 3.0$, the liquid jet is affected by the vertical wall lightly, which could be seen in Figs. 8 and 9; so in this figure, the jet is considered to point toward the vertical wall when the angle between the jet direction and the x-axis is less than 30°. Of course, it is noticeable that the liquid jet almost points downward near the free surface, which is similar to the law of Sec. IV B 1. In region D, the horizontal wall has only a slight effect on the jet direction of the bubble, and so the jet direction mainly depends on the free surface and the vertical wall; in this region, the jet points downward because of the extraordinary interaction among the bubble, free surface, and vertical wall[6,17,27] as the collapsing bubble profile shows in Fig. 12(c). When the bubble is close to the corner (region A), the effect of the free surface is relatively lighter, and the existence of buoyancy means that the Bjerknes force in the vertical direction is largely counteracted. Under this condition, the vertical wall has a big effect on the bubble, and so the bubble jet is directed to the vertical solid wall. A little further from the vertical solid wall, the jet direction depends on the distance parameter γ_h. When the bubble is close to the horizontal wall (region B), the direction of the bubble jet is dominated by the effect of the horizontal wall, leading to a downward jet. As γ_h reaches 2.0, as a result of the balance of forces in the vertical direction, no bubble jet forms in the vertical direction, and the bubble would go on dilating (region E) or generates an almost horizontal jet (region A) according to different γ_v. An analogous phenomenon in region E was observed by Blake *et al.*[16] in their numerical simulations, and the corresponding typical collapsing bubble shape can be seen in Fig. 12(c). As γ_v continues to increase, in region C the buoyancy becomes greater than the Bjerknes force in the vertical direction, and the jet is directed obliquely upward as Fig. 12(c). When γ_v reaches about 3.5 (region F), the Bjerknes force from the horizontal wall decreases a lot, but that from the free surface increases obviously; similarly to the region E, the Bjerknes force in the vertical direction is balanced by the buoyancy, and so no liquid jet forms in the stage of collapsing bubble. After the bubble collapses to its minimum volume, it continues to expand and enters the next cycle, for the internal pressure becomes much stronger than the external pressure at this time. The bubble profiles at its minimum volume (region E and F) are shown in Fig. 12(c). It can be seen that there exits some differences in the shape of bubble between that in the region E and F. As an explanation for the difference, the effect of the Bjerknes force from the free surface generates a wide region with high pressure,[27] which squashes the bubble combined the buoyancy; however, the Bjerknes force from the bottom wall is relatively smaller than the difference in the internal and external pressure, and so the joint force exerted on the bubble in the horizontal direction is larger than that in the vertical direction, causing the bubble to be pushed horizontally.

The change in jet angles with γ_v under the condition of different γ_h is plotted in Fig. 12(b). The jet direction eventually becomes vertical with the increase in γ_v under the condition $\alpha \neq 0$. What is different from Fig. 10 is the appearance of negative jet angles as a result of the effect of buoyancy; we can see the jet angle with the greater γ_h tends to be smaller at $\alpha < 0$ owing to the lighter effect of the bottom wall. Those data in the black box can be regarded as the jet pointing the vertical wall [region A in Fig. 12(a)] as mentioned above, and this may seem to be very useful in some projects such as unblocking channels. As for the calculated results at $\gamma_h > 4.0$, we choose not to show them because the angles are all 90° as explained in region D. Note that the jet angle of the bubble near the free surface ($\gamma_h = 4.0$) reaches 90° at a smaller value of γ_v than near the horizontal wall. The same regularity can be acquired from Fig. 12(a): when $\gamma_h = 3.5$, no obvious jet exists in the vertical direction, and the jet disappears only when γ_v reaches 3.5, whereas the jet disappears when

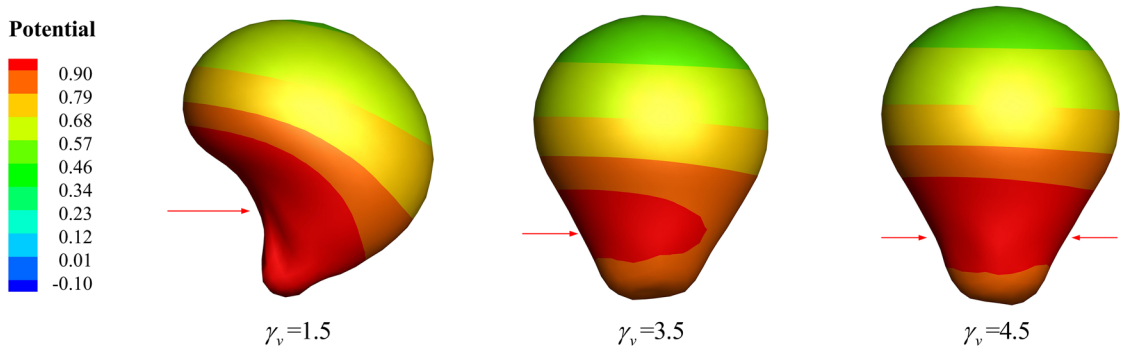

FIG. 13. Jet shapes of different γ_V when $\gamma_h = 1.0$. The dimensionless buoyancy parameter $\delta = 0.4$; the corresponding dimensionless moments are 2.257, 2.059, 2.093; different colors denote different potentials, as presented on the left of the image; the red arrows represent the tendency of the bubble jet.

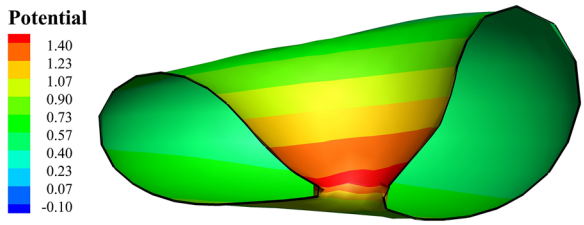

FIG. 14. Jet shape at the time of jet impact under the conditions γ_v = 4.0, γ_h = 5.0. The dimensionless buoyancy parameter δ = 0.4; different colors denote different potentials, as presented on the left of the image.

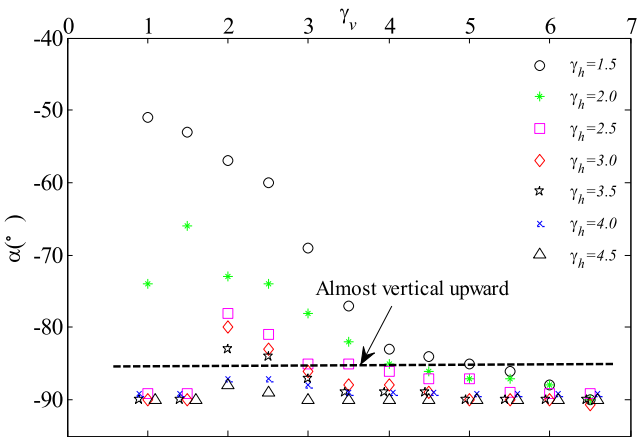

FIG. 15. Jet angles with respect to γ_v for different γ_h. The dimensionless buoyancy parameter δ = 0.4; seven different symbols denote different dimensionless distance parameters between the bubble and horizontal wall, with black circles, green asterisks, pink squares, red diamonds, black pentagrams, blue crosses, and black triangles denoting the jet angle when γ_h equals 1.5, 2.0, 2.5, 3.0, 3.5, 4.0, and 4.5, respectively; the area below the dashed line represents an almost-upward jet.

γ_v reaches 6.0 in the vicinity of the bottom wall. Near the horizontal wall, the range of influence of the vertical wall on the jet direction is roughly equal to the range (about 5.5) under the condition of a vertical wall alone. However, near the free surface, the range of influence decreases significantly (to about 2.0). Hence, the existence of the free surface can decrease the influence of the vertical wall on the jet direction, and the effect of the vertical wall on the jet direction decreases as the distance between the bubble and the free surface decreases.

b. Jet characteristics of bubbles under the action of obvious buoyancy (δ = 0.4). Figure 13 shows the jet shape of the bubble at some typical distances when γ_h = 1.0. The bubble has no tendency to produce an obvious jet when the distance parameter γ_h = 1.0, but appears like a funnel, because the buoyancy effect is sufficient to counteract the Bjerknes force in the vertical direction at this distance; and we can see the bubble is also influenced by the vertical wall obviously at γ_v = 1.5, which makes the bubble nearly assume a moon shape. Figure 15 depicts the change in jet angles with γ_v for different values of γ_h. In the vertical direction, the jet will point toward the bottom ($\alpha < -45°$) when the bubble is very close to the free surface (γ_h = 5.0) owing to the same reason as the region D of Fig. 12(a), as shown in Fig. 14 (free surface is not displayed). At this δ, only when the γ_h is greater than 4.5 does the liquid jet points vertical downward (those data are not shown), and so it can be seen that the number of these cases decreases because of the obvious buoyancy. Similarly, we also observe a jump in the jet angle when γ_v is relatively small, but the jump does not occur when γ_h = 1.5, a result of the strong induction effect of the horizontal wall. From these data in Fig. 15, the liquid jets almost all tend to be directed upward except some cases near the vertical wall (γ_v < 2.0). So in conclusion, under the condition δ = 0.4, buoyancy begins to dominate the jet direction in most areas.

c. Analysis of the influence of buoyancy on the jet characteristics. To investigate the influence of buoyancy, some cases are considered under the condition δ = 0.6. When the bubble is very close to the free surface (γ_h = 5.0), the bubble generates two jets under the action of buoyancy and the Bjerknes force, as shown in Fig. 16, which may be the symbol that the hydrostatic pressure difference between the upper and lower part of the bubble is almost the same as that of the high pressure zone[15] between the bubble and free surface. In other areas, the bubble points toward the free surface ($\alpha < -45°$) as a result of the large buoyancy effect and the relatively small effect of the boundaries. Hence, we can conclude that after the δ reaches about 0.6, the bubble jet almost will not have obvious impacts on the bottom.

Figure 17 shows the change in jet angles with respect to γ_v near the horizontal solid wall for different values of δ when the γ_h equals 1.5. The bubble jet tends to point toward the bottom ($\alpha > 0$) under the condition of small buoyancy (δ = 0.2) and point toward the free surface ($\alpha < 0$) under the condition of large buoyancy (δ = 0.4, 0.6). When the jet angle is positive, the Bjerknes force in the vertical

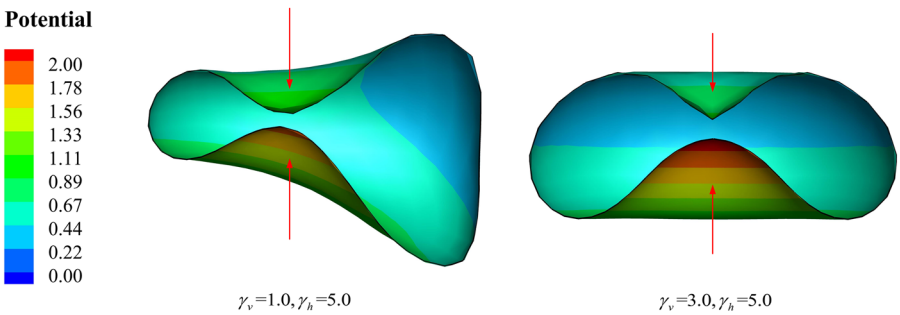

FIG. 16. Jet shape under typical conditions. The corresponding dimensionless moments are 1.717 and 1.658, respectively; different colors denote different potentials, as presented on the left of the image; the red arrows represent the tendency of the bubble jet. γ_v = 1.0, γ_h = 5.0, γ_v = 3.0, γ_h = 5.0.

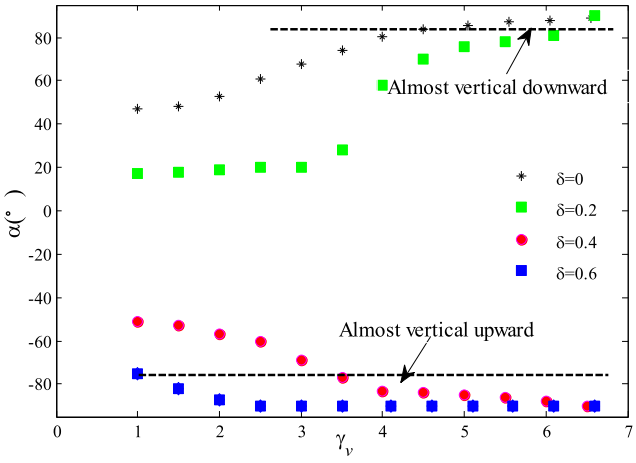

FIG. 17. Jet angles changing with γ_v when γ_h = 1.5 for different δ. Four different symbols denote different dimensionless buoyancy parameters, with black asterisks, green squares, pink circles, and blue squares denoting the jet angle when δ equals 0, 0.2, 0.4, and 0.6, respectively; the area above the top line and below the bottom line represents an almost-vertical jet.

direction is greater than the buoyancy. As the δ increases, the joint force in the vertical direction reduces, leading to the liquid jet directed toward the horizontal wall, and so the jet angle reaches 90° at a smaller value of γ_v under the condition of smaller buoyancy. When the jet angle is negative, the Bjerknes force in the vertical direction is smaller than the buoyancy. As the δ increases, the joint force in the vertical direction increases, leading to the liquid jet directed upward, and so the jet angle reaches −90° at a smaller value of γ_v under the condition of larger buoyancy. For δ = 0, 0.2, 0.4, and 0.6, the bubble jet becomes almost vertical when the γ_v is 6.0, 6.0, 4.0, and 2.0, respectively, that is, when δ reaches 0.6, the range of influence of the vertical wall on the jet direction is reduced by about two-thirds compared with the condition δ = 0. Therefore, there is no need to investigate further increases in δ. As analyzed in Figs. 10, 12, and 15, the bubble jets show much different characteristics at each δ. From them, we can know that in the presence of the liquid jet the jet angle rotates counterclockwise at the fixed value of γ_v and γ_h with the increase in δ until the angle approaches 90°, which is the result of the joint force gradually rotating counterclockwise.

V. CONCLUSIONS

This paper has described the jet characteristics of bubbles near a mixed boundary. By calculating the jet angles and velocities under different conditions, we have analyzed the influence of distance parameters and the buoyancy parameter on the jet characteristics, which are related to underwater explosions and other important engineering applications.

First, we investigated the range of influence of a vertical wall on the direction of the bubble jet and found that this range decreases as δ increases. Near the wall, there exists a jump in the jet angle with respect to γ_v. As for the jet velocity, as expected, it decreases with an increase in the distance between the bubble and the wall until the effect of the wall is negligible.

With mixed boundaries, we verified the feasibility of our numerical model through a comparison with experimental results, and then studied the jet direction under different values of δ. In the case of negligible buoyancy, the bubble jet tends to point downward in most areas ($\alpha > 45°$). The discrepancy of jet angles under the same γ_v decreases with the increase of γ_v, and after γ_v reaches 4.5, the jet angles at different positions have no obvious difference, but generally approach 90°. In the vertical direction, the jet velocity at mid water depths (about 3.0) tends to be higher than that in other areas, and the jet velocity of bubbles near the bottom tends to be higher than that near the free surface. In the horizontal direction, the jet velocity reaches its peak close to the vertical wall and decreases with an increase in γ_v. In addition, the existence of mixed boundaries causes the jet velocity to be much lower than with a vertical wall alone.

Under the influence of small buoyancy (δ = 0.2), the direction of the bubble jet exhibits obvious discrepancies in different areas depending on γ_v and γ_h. The jet directions in the whole domain were identified [see Fig. 12(a)]. Compared with the condition of an infinite vertical wall alone, the range of influence of the vertical wall on the jet direction decreases in the presence of the free surface, and the effect of the free surface on the jet direction is greater than that of the horizontal wall. Under the action of obvious buoyancy (δ = 0.4), the buoyancy force dominates the jet direction in almost the whole area. No jet is generated in the vicinity of the bottom (γ_h = 1.0). After γ_h reaches 2.0, the change in jet angle with respect to γ_v has a jump when the bubble is close to the vertical wall, which is similar to the condition of the infinite wall alone. However, this jump disappears when γ_h is small ($\gamma_h \leq 1.5$). When δ = 0.6, the jet points almost upward in all cases owing to the strong buoyancy, and near the corner, the jet becomes vertical within about one-third of the range required with negligible buoyancy, and so the condition with larger values of δ need not be studied.

ACKNOWLEDGMENTS

This work was supported by the National Key R&D Program of China (Grant No. 2018YFC0308900), the Industrial Technology Development Program (Grant Nos. JCKY2017604C002 and JCKY2018604C010), and the National Natural Science Foundation of China (Grant No. 11872158). The authors are grateful to Dr. Liu Yunlong and Dr. Cui Pu for the help with the programming and experiments.

REFERENCES

[1] S. P. Wang, A. M. Zhang, Y. L. Liu, S. Zhang, and P. Cui, "Bubble dynamics and its applications," J. Hydrodyn. **30**, 975 (2018).
[2] J. R. Blake and D. C. Gibson, "Cavitation bubbles near boundaries," Annu. Rev. Fluid Mech. **19**, 99 (1987).
[3] G. L. Chahine, C. T. Hsiao, and R. Raju, "Scaling of cavitation bubble cloud dynamics on propellers," Fluid Mech. Its Appl. **106**, 345 (2014).
[4] G. Q. Chen, A. M. Zhang, and X. Huang, "On the interaction between bubbles and the free surface with high density ratio 3D lattice Boltzmann method," Theor. Appl. Mech. Lett. **8**, 252 (2018).
[5] Q. X. Wang, "The evolution of a gas bubble near an inclined wall," Theor. Comput. Fluid Dyn. **12**, 29 (1998).
[6] Q. X. Wang, K. S. Yeo, B. C. Khoo, and K. Y. Lam, "Strong interaction between a buoyancy bubble and a free surface," Theor. Comput. Fluid Dyn. **8**, 73 (1996).

[7]B. Ji, X. Luo, R. Arndt, and Y. Wu, "Numerical simulation of three dimensional cavitation shedding dynamics with special emphasis on cavitation–vortex interaction," Ocean Eng. **87**, 64 (2014).
[8]S. Eiamsa-Ard, S. Rattanawong, and P. Promvonge, "Turbulent convection in round tube equipped with propeller type swirl generators," Int. Commun. Heat Mass Transfer **36**, 357 (2009).
[9]D. Benjamin, V. Wim, R. Jan, M. Philippe, and V. Michel, "Role of the channel geometry on the bubble pinch-off in flow-focusing devices," Phys. Rev. Lett. **100**, 034504 (2008).
[10]A. Ziolkowski, "A method for calculating the output pressure waveform from an air gun," Geophys. J. R. Astron. Soc. **21**, 137 (1970).
[11]S. Zhang, S. P. Wang, A. M. Zhang, and P. Cui, "Numerical study on motion of the air-gun bubble based on boundary integral method," Ocean Eng. **154**, 70 (2018).
[12]A. Ziolkowski, "Measurement of air-gun bubble oscillations," Geophysics **63**, 2009 (1998).
[13]A. M. Zhang, P. Cui, J. Cui, and Q. X. Wang, "Experimental study on bubble dynamics subject to buoyancy," J. Fluid Mech. **776**, 137 (2015).
[14]P. Cui, A. M. Zhang, S. Wang, and B. C. Khoo, "Ice breaking by a collapsing bubble," J. Fluid Mech. **841**, 287 (2018).
[15]S. Zhang, S. Wang, and A. M. Zhang, "Experimental study on the interaction between bubble and free surface using a high-voltage spark generator," Phys. Fluids **28**, 032109 (2016).
[16]J. R. Blake, B. B. Taib, and G. Doherty, "Transient cavities near boundaries. Part 1. Rigid boundary," J. Fluid Mech. **170**, 479 (1986).
[17]J. R. Blake, B. B. Taib, and G. Doherty, "Transient cavities near boundaries. Part 2. Free surface," J. Fluid Mech. **181**, 197 (2006).
[18]A. M. Zhang, P. Cui, and S. Wang, "Experiments on bubble dynamics between a free surface and a rigid wall," Exp. Fluids **54**, 1602 (2013).
[19]S. Wang, W. Chu, and A. M. Zhang, "Experimental study on bubble pulse features under the combined action of horizontal and vertical walls," China Ocean Eng. **28**, 293 (2014).
[20]A. Dadvand, B. C. Khoo, M. T. Shervani-Tabar, and S. Khalilpourzary, "Boundary element analysis of the droplet dynamics induced by spark-generated bubble," Eng. Anal. Boundary Elem. **36**, 1595 (2012).
[21]S. Li, R. Han, A. M. Zhang, and Q. X. Wang, "Analysis of pressure field generated by a collapsing bubble," Ocean Eng. **117**, 22 (2016).
[22]Q. X. Wang, "Numerical simulation of violent bubble motion," Phys. Fluids **16**, 1610 (2004).
[23]B. B. Li, H. C. Zhang, H. Bing, and L. Jian, "Numerical study of ambient pressure for laser-induced bubble near a rigid boundary," Sci. China: Phys., Mech. Astron. **55**, 1291 (2012).
[24]R. Han, L. Tao, A. M. Zhang, and S. Li, "A three-dimensional modeling for coalescence of multiple cavitation bubbles near a rigid wall," Phys. Fluids **31**, 062107 (2019).
[25]Z. Tian, Y. Liu, S. Wang, A. M. Zhang, and Y. Kang, "Dynamic response of floating body subjected to underwater explosion bubble and generated waves with 2D numerical model," Comput. Modell. Eng. Sci. **118**, 397 (2019).
[26]A. M. Zhang and B. Y. Ni, "Influences of different forces on the bubble entrainment into a stationary Gaussian vortex," Sci. China: Phys., Mech. Astron. **56**, 2162 (2013).
[27]Q. X. Wang, "The motion of a 3D toroidal bubble and its interaction with a free surface near an inclined boundary," Phys. Fluids **28**, 122101 (2016).
[28]P. Koukouvinis, M. Gavaises, O. Supponen, and M. Farhat, "Numerical simulation of a collapsing bubble subject to gravity," Phys. Fluids **28**, 032110 (2016).
[29]T. Li, A.-M. Zhang, S.-P. Wang, S. Li, and W.-T. Liu, "Bubble interactions and bursting behaviors near a free surface," Phys. Fluids **31**, 042104 (2019).
[30]T. Li, S. Wang, S. Li, and A.-M. Zhang, "Numerical investigation of an underwater explosion bubble based on FVM and VOF," Appl. Ocean Res. **74**, 49 (2018).
[31]L. T. Liu, X. L. Yaoa, A. M. Zhanga, and Y. Y. Chen, "Numerical analysis of the jet stage of bubble near a solid wall using a front tracking method," Phys. Fluids **29**, 012105 (2017).
[32]G.-Q. Chen, X. Huang, A.-M. Zhang, and S.-P. Wang, "Simulation of three-dimensional bubble formation and interaction using the high-density-ratio lattice Boltzmann method," Phys. Fluids **31**, 027102 (2019).
[33]Y. Tagawa and I. R. Peters, "Bubble collapse and jet formation in corner geometries," Phys. Rev. Fluids **3**, 081601 (2018).
[34]P. Cui, A. M. Zhang, and S. P. Wang, "Small-charge underwater explosion bubble experiments under various boundary conditions," Phys. Fluids **28**, 117103 (2016).
[35]M. A. Maiga, O. Coutier-Delgosha, and D. Buisine, "A new cavitation model based on bubble-bubble interactions," Phys. Fluids **30**, 123301 (2018).
[36]S. Zhang, A. M. Zhang, S. P. Wang, and J. Cui, "Dynamic characteristics of large scale spark bubbles close to different boundaries," Phys. Fluids **29**, 092107 (2017).
[37]S. Li, B. C. Khoo, A. M. Zhang, and S. Wang, "Bubble-sphere interaction beneath a free surface," Ocean Eng. **169**, 469 (2018).
[38]S. Li, Y. B. Li, and A. M. Zhang, "Numerical analysis of the bubble jet impact on a rigid wall," Appl. Ocean Res. **50**, 227 (2015).
[39]A. M. Zhang and Y. L. Liu, "Improved three-dimensional bubble dynamics model based on boundary element method," J. Comput. Phys. **294**, 208 (2015).
[40]J. P. Best and A. Kucera, "A numerical investigation of non-spherical rebounding bubbles," J. Fluid Mech. **245**, 137 (2006).
[41]S. Li, A.-M. Zhang, R. Han, and Q. Ma, "3D full coupling model for strong interaction between a pulsating bubble and a movable sphere," J. Comput. Phys. **392**, 713 (2019).
[42]Y. L. Zhang, K. S. Yeo, B. C. Khoo, and C. Wang, "3D jet impact and toroidal bubbles," J. Comput. Phys. **166**, 336 (2001).
[43]Q. X. Wang and K. Manmi, "Three dimensional microbubble dynamics near a wall subject to high intensity ultrasound," Phys. Fluids **26**, 032104 (2014).
[44]A. M. Zhang, W. S. Yang, C. Huang, and F. R. Ming, "Numerical simulation of column charge underwater explosion based on SPH and BEM combination," Comput. Fluids **71**, 169 (2013).
[45]A. Dadvand, B. C. Khoo, and M. T. Shervani-Tabar, "A collapsing bubble-induced microinjector: An experimental study," Exp. Fluids **46**, 419 (2009).
[46]F. G. Hammitt, "Discussion: "Interaction between an oscillating bubble and a free surface"," J. Fluids Eng. **99**, 709 (1977).
[47]C. F. Naude, "On the mechanism of cavitation damage by non-hemispherical cavities collapsing in contact with a solid boundary," J. Basic Eng. **83**, 648 (1960).
[48]D. Obreschkow, P. Kobel, and N. Dorsaz, "Cavitation bubble dynamics inside liquid drops in microgravity," Phys. Rev. Lett. **97**, 094502 (2006).
[49]S. Li, A. M. Zhang, S. Wang, and R. Han, "Transient interaction between a particle and an attached bubble with an application to cavitation in silt-laden flow," Phys. Fluids **30**, 082111 (2018).
[50]B. Silvano and G. B. Cannelli, "Implosion of an underwater spark-generated bubble and acoustic energy evaluation using the Rayleigh model," J. Acoust. Soc. Am. **111**, 2594 (2002).
[51]C. K. Turangan, G. P. Ong, E. Klaseboer, and B. C. Khoo, "Experimental and numerical study of transient bubble-elastic membrane interaction," J. Appl. Phys. **100**, 054910 (2006).
[52]J. R. Blake, Y. Tomita, and R. P. Tong, "The art, craft and science of modelling jet impact in a collapsing cavitation bubble," Appl. Sci. Res. **58**, 77 (1997).
[53]E. Klaseboer, K. C. Hung, C. Wang, C. W. Wang, B. C. Khoo, P. Boyce, S. Debono, and H. Charlier, "Experimental and numerical investigation of the dynamics of an underwater explosion bubble near a resilient/rigid structure," J. Fluid Mech. **537**, 387 (2005).
[54]P. B. Robinson and J. R. Blake, "Interaction of cavitation bubbles with a free surface," J. Appl. Phys. **89**, 8225 (2001).
[55]L. K. Wang, Z. F. Zhang, and S. P. Wang, "Pressure characteristics of bubble collapse near a rigid wall in compressible fluid," Appl. Ocean Res. **59**, 183 (2016).
[56]E.-A. Brujan, T. Noda, A. Ishigami, T. Ogasawara, and H. Takahira, "Dynamics of laser-induced cavitation bubbles near two perpendicular rigid walls," J. Fluid Mech. **841**, 28 (2018).
[57]Z. Li, L. Sun, Z. Zhi, and J. Dong, "Some dynamical characteristics of a non-spherical bubble in proximity to a free surface," Acta Mech. **223**, 2331 (2012).
[58]A. Pearson, E. Cox, J. R. Blake, and S. R. Otto, "Bubble interactions near a free surface," Eng. Anal. Boundary Elem. **28**, 295 (2004).